MetMAb, the One-Armed 5D5 Anti-c-Met Antibody, Inhibits Orthotopic Pancreatic Tumor Growth and Improves Survival

Hongkui Jin,[1] Renhui Yang,[1] Zhong Zheng,[1] Mally Romero,[1] Jed Ross,[2] Hani Bou-Reslan,[2] Richard A.D. Carano,[2] Ian Kasman,[3] Elaine Mai,[4] Judy Young,[4] Jiping Zha,[3] Zemin Zhang,[5] Sarajane Ross,[1] Ralph Schwall,[1] Gail Colbern,[1] and Mark Merchant[1]

Departments of [1]Translational Oncology, [2]Tumor Biology and Angiogenesis, [3]Pathology, [4]Assay and Automation Technology, and [5]Bioinformatics, Genentech, Inc., South San Francisco, California

Abstract

The hepatocyte growth factor (HGF) and its receptor, c-Met, have been implicated in driving proliferation, invasion, and poor prognosis in pancreatic cancer. Here, we investigated the expression of HGF and c-Met in primary pancreatic cancers and described *in vitro* and *in vivo* models in which MetMAb, a monovalent antibody against c-Met, was evaluated. First, expression of *HGF* and *MET* mRNA was analyzed in 59 primary pancreatic cancers and 51 normal samples, showing that both factors are highly expressed in pancreatic cancer. We next examined HGF responsiveness in pancreatic cancer lines to select lines that proliferate in response to HGF. Based on these studies, two lines were selected for further *in vivo* model development: BxPC-3 (c-Met$^+$, HGF$^-$) and KP4 (c-Met$^+$, HGF$^+$) cells. As BxPC-3 cells are responsive to exogenous HGF, s.c. tumor xenografts were grown in a paracrine manner with purified human HGF provided by osmotic pumps, wherein MetMAb treatment significantly inhibited tumor growth. KP4 cells are autocrine for HGF and c-Met, and MetMAb strongly inhibited s.c. tumor growth. To better model pancreatic cancer and to enable long-term survival studies, an orthotopic model of KP4 was established. MetMAb significantly inhibited orthotopic KP4 tumor growth in 4-week studies monitored by ultrasound and also improved survival in 90-day studies. MetMAb significantly reduced c-Met phosphorylation in orthotopic KP4 tumors with a concomitant decrease in Ki-67 staining. These data suggest that the HGF/c-Met axis plays an important role in the progression of pancreatic cancer and that targeting c-Met therein may have therapeutic value. [Cancer Res 2008;68(11):4360–8]

Introduction

Pancreatic cancer is a highly lethal disease with a rising incidence (1). Worldwide, over 200,000 people die annually of pancreatic cancer, making it the fourth leading cause of cancer death in the United States (2, 3). Prognosis has not been improved substantially over the past few decades and 5-year survival rates remain <5% (4–6). Therefore, novel treatment strategies for pancreatic cancer are urgently needed.

The hepatocyte growth factor (HGF)/c-Met pathway has been linked to the cancer progression by driving proliferation, motility, invasion, and angiogenesis (7–10) and further has been linked to malignancy in pancreatic cancer (11–20). The c-Met receptor is overexpressed in pancreatic cancer cells, whereas tumor-associated fibroblasts produce HGF in a paracrine manner (11, 13–20). HGF/c-Met signaling not only stimulates growth, locomotion, and invasion of pancreatic cancer cells *in vitro* but also promotes pancreatic tumor growth and invasion and metastasis *in vivo* (16–26).

We have developed MetMAb, a monovalent monoclonal antibody (mAb) against c-Met, which blocks HGF binding to c-Met and subsequent pathway activation. MetMAb and other anti-HGF antibodies have shown potent activity in the U-87 MG autocrine glioblastoma tumor model (27–29); however, it had previously not been evaluated in pancreatic cancer models. As prognosis in pancreatic cancer has been linked to ligand-driven c-Met activity, modeling ligand-driven activation in animals would be ideal. Unfortunately, mouse HGF does not activate human c-Met (30, 31), making it essential to either use autocrine models or generate engineered human HGF paracrine models to evaluate the role of ligand in driving tumor progression.

In the present study, we investigated expression of HGF and c-Met by mRNA in primary pancreatic samples and explore functionality of HGF/c-Met signaling in cell-based and animal models to validate this pathway as a therapeutic target in pancreatic cancer and to explore efficacy of MetMAb. We describe the development of two novel HGF-driven s.c. pancreatic xenograft models: a BxPC-3 paracrine-driven model using osmotic pumps to provide exogenous human HGF and a KP4 autocrine-driven model, both of which showed responses to MetMAb. We further developed KP4 in an orthotopic setting, allowing us to explore long-term survival studies and the efficacy of MetMAb in a HGF-driven model. Together, these studies help further our understanding of the role of HGF/c-Met signaling in pancreatic cancer and help to validate MetMAb as a promising therapeutic against HGF/c-Met–driven cancers.

Materials and Methods

Cell lines. The KP4 pancreatic ductal carcinoma cell line was obtained from the Riken BioResource Center Cell Bank (cell line RCB1005). The Capan-1 cell line was obtained from the German Collection of Microorganisms and Cell Cultures. The BxPC-3, AsPC-1, HPAC, CFPAC-1, and Su.86.86 pancreatic adenocarcinoma cell lines and the A549 non–small cell lung cancer cell line were obtained from the American Type Culture Collection.

Immunoprecipitation and immunoblotting. Cells were cultured overnight in serum-free medium and then pretreated with different concentrations of MetMAb at 37°C for 1 h and then with or without 1 nmol/L HGF (~100 ng/mL) for 15 min. Cells were lysed with lysis buffer (Cell Signaling Technology, Inc.), supplemented with 1 mmol/L phenylmethylsulfonyl fluoride, additional protease inhibitor cocktail, and

Note: Supplementary data for this article are available at Cancer Research Online (http://cancerres.aacrjournals.org/).

Requests for reprints: Hongkui Jin, Department of Translational Oncology, Genentech, Inc., 1 DNA Way, South San Francisco, CA 94080. Phone: 650-225-1314; Fax: 650-467-7991; E-mail: hkj@gene.com.

doi:10.1158/0008-5472.CAN-07-5960

phosphatase inhibitor cocktail I and II (Sigma, Inc.). Cell lysates were incubated on ice for 1 h and then centrifuged at 14,000 × *g* for 5 min and supernatants were collected. Analysis of tumor proteins was done in a similar fashion; however, tumors first were homogenized using a glass Dounce homogenizer. Protein concentrations were determined using the BCA Protein Assay kit (Pierce, Inc.) and samples were immunoblotted. For immunoprecipitations, 6 mg of tumor lysates were incubated with C-28 anti-human c-Met polyclonal antibody (Santa Cruz Biotechnology, Inc.) conjugated to agarose beads at 4°C overnight with rotation. The beads were washed thrice with lysis buffer at 4°C followed by resuspension in 1× Novex Tris-Glycine SDS Running Buffer (Invitrogen, Inc.) containing 2.5% (w/v) β-mercaptoethanol. Samples were then analyzed by SDS-PAGE and immunoblotting. Antibodies used include the mouse anti-human c-Met DL-21 and mouse anti-phosphotyrosine mAb 4G10 (Upstate Biotechnology/Millipore, Inc.); rabbit anti-human c-Met C-12 polyclonal antibody (Santa Cruz Biotechnology); and anti-Akt, anti-p44/42 mitogen-activated protein kinase (MAPK), anti-p70 S6 kinase (p70S6K), anti-growth factor receptor binding protein 2-associated binder-1 (Gab-1), rabbit anti-phospho-c-Met ($Tyr^{1234/1235}$), anti-phospho-Akt (Ser^{473}), anti-phospho-p44/42 MAPK (Thr^{202}/Tyr^{204}), anti-phospho-p70S6K (Thr^{389}, 1A5), and anti-phospho-Gab-1 (Tyr^{307}; Cell Signaling Technology), all used according to the manufacturer's recommendations. Goat anti-mouse IRDye800 (Rockland Immunochemicals, Inc.) and goat anti-rabbit Alexa Fluor 680 (Molecular Probes, Inc.) were used as secondary antibodies. Immunoblots were imaged and protein levels were quantified and normalized to β-actin levels using an Odyssey imager (LI-COR Biosciences).

Cell viability assays. Cancer cells were washed once with PBS, resuspended in serum-free medium, counted, and then added to 96-well plates (2,500 per well). Cell plates were with MetMAb ± human HGF (1 nmol/L). Three-day Alamar Blue assays were performed according to the manufacturer's recommendations (BioSource International). IC_{50} values were determined by nonlinear regression analysis with a four-variable model (KaleidaGraph, Synergy Software).

Animals. Female *nu/nu* nude mice (Charles River Laboratories) were acclimated to the animal housing facility for at least 1 wk before studies. All experimental procedures conformed to the guiding principles of the American Physiology Society and were approved by Genentech's Institutional Animal Care and Use Committee.

S.c. xenograft models. For the BxPC-3 human HGF pump model, there were three groups: group 1, mice received 5 million BxPC-3 cells via s.c. inoculation in HBSS a day after they were implanted i.p. with Alzet osmotic pumps (model 1002) containing human HGF in dextran sulfate, resulting in a HGF dose of ~2.4 mg/kg/d (n = 24); group 2, same as group 1, however, pumps contained only dextran sulfate carrier (n = 5); and group 3, mice received BxPC-3 cells as above but no pumps (n = 5). Tumors from group 1 were allowed to become established to ~140 mm^3 and then were separated into two subgroups of nine animals each: vehicle {MetMAb buffer [10 mmol/L histidine succinate, 4% trehalose dihydrate, 0.02% polysorbate 20 (pH 5.7)] diluted in 1× PBS}, twice weekly at 100 μL dosed i.p., and MetMAb (30 mg/kg, i.p., twice weekly). Tumor dimensions were measured by digital caliper, and tumor volumes were calculated as length × $(width)^2$ / 2. Osmotic pumps were replaced every 12 to 14 d.

For the KP4 model, mice were injected s.c. with human KP4 pancreatic cancer cells (10 million in HBSS per mouse). When tumors reached ~150 mm^3, mice were randomized and treated with vehicle or MetMAb (30 mg/kg, i.p., twice weekly) for 2 wk. Pilot studies showed that this dose inhibited tumor growth without adversely affecting body weight and was used to ensure sufficient exposure.

Orthotopic xenograft model. Mice were anesthetized with i.p. injection of 80 mg/kg ketamine (Aveco Co., Inc.) and 10 mg/kg xylazine (Rugby Laboratories, Inc.). A small (~1 cm) lateral subcostal laparotomy was performed. Two million KP4 cells, suspended in 20 μL HBSS, were injected beneath the capsule of the pancreas. Following cell injection, bleeding or leakage of cells from the pancreas was stopped by applying Matrigel (BD Biosciences) to the site of injection, and the abdominal wall and skin were closed.

Pretreatment ultrasound imaging was performed 12 d after orthotopic injection of tumor cells. Ultrasound analysis allowed for selection of 39 of 50 mice to be divided into two groups with a similar mean tumor volumes, and treatment with vehicle (n = 19) or MetMAb (30 mg/kg, i.p., twice weekly; n = 20) began. Two weeks later, mice were again imaged by ultrasound, and tumor volume was assessed. Treatment continued for 11 wk or until animal death. Survival was followed for 90 d after cell injection.

To assess short-term treatment on survival, the above protocol was followed; however, animals were randomized blindly into two groups (n = 24 per group) with ultrasound assessment in a subset of five mice from each group (vehicle group = 9.93 ± 3.74 mm^3 and MetMAb group = 10.29 ± 4.81 mm^3) and then mice were treated with vehicle or MetMAb (30 mg/kg, i.p., twice weekly) for 2 wk (n = 24 per group) and survival was monitored for 90 d after cell injection.

To assess MetMAb efficacy on larger orthotopic tumors, the above protocol was modified by increasing both the number of KP4 cells injected, from 2 to 3 million cells (in 20 μL), and the time to initial ultrasound assessment, from 12 to 16 d. Thirty animals were implanted with KP4 cells and then assessed by ultrasound on day 16. Twenty-six of 30 animals were divided into two groups (n = 13 per group) and treated with vehicle or MetMAb (30 mg/kg, i.p., twice weekly) for 2 wk. Following treatment, ultrasound imaging was repeated and mice were euthanized. Tumors were removed, weighed, and fixed in 10% buffered formalin for immunohistochemical studies.

To generate orthotopic tumors for evaluation of c-Met phosphorylation, the above protocol was followed; however, mice were randomly treated with MetMAb (30 mg/kg, i.p.) or vehicle on day 14 after tumor cell inoculation. Twenty-four and 48 h after treatment, tumors were removed, flash frozen in liquid nitrogen, and stored at −80°C until processed for evaluation of c-Met phosphorylation.

Ultrasound imaging. Tumor volume assessments were made by high-resolution micro-ultrasound imaging as described previously (32, 33). Micro-ultrasound imaging was performed with a VisualSonics Vevo 770 microimaging system. During the imaging procedure, mice were anesthetized with 2% isoflurane vaporized in medical air. Animal temperature was monitored and maintained at 37°C with a heated imaging platform. Tumor volume was estimated by defining three-dimensional regions of interest using the VisualSonics image analysis software package.

Immunohistochemistry. Fixed xenograft tumors (n = 4 per group) were processed and embedded in paraffin and sectioned at 3 μm onto slides. After deparaffinization and rehydration, sections were processed for standard H&E processing and Ki-67 immunohistochemical analysis as described previously (34).

Dorsal skin window chamber model. Mice were anesthetized with ketamine and xylazine as described above. The surgical procedure was described previously (35). Two days after implantation of the dorsal chamber, a piece (1 mm in diameter) of KP4 tumor was implanted onto the fascia at the center of the chamber. When tumors reached the desired size (~4 mm diameter), animals were randomized to receive i.p. injection of MetMAb (30 mg/kg twice weekly) or vehicle (n = 4 per group). Tumor size was observed and recorded with a light microscope before and after each treatment. To examine the effect of treatment on tumor vasculature, animals were i.v. injected with 100 μL of FITC-dextran (molecular weight, 2 million; 10 mg/mL), and animals, under isoflurane anesthesia, were immediately imaged with a Zeiss LSM510 laser scanning confocal microscope (488 nm krypton-argon laser). Tumor regions were optically sectioned, and a maximum intensity projection was generated using Zeiss LSM software (v3.2). Vascular area measurements were calculated from these images using ImageJ 1.34.[6] Vascular area was calculated from the total number of pixels above set threshold. Vascular density is expressed as the percent vascular area/image area.

Statistical analysis. Results are expressed as mean ± SE. To assess differences in tumor size and vascular volume between two groups, Student's t test was performed. Survival was compared by log-rank (Mantel-Cox) test.

[6] http://rsb.info.nih.gov/ij

Results

***HGF* and *MET* expression in pancreatic cancer.** To explore expression levels of HGF and c-Met in pancreatic cancer, we obtained Affymetrix HG-U133 chip-based microarray data for 59 human pancreatic adenocarcinomas and 51 normal pancreatic tissue samples from Gene Logic. *HGF* showed higher expression in pancreatic adenocarcinomas than normal controls (P = 1.44e−08) with a higher degree of variation of expression (Fig. 1*A*). Twenty-seven of 59 (45.8%) tumors had *HGF* levels greater than twice the mean of normal, suggesting that in nearly half of pancreatic cancers HGF is expressed to a greater extent. Pancreatic adenocarcinomas also showed much higher expression of *MET* than normal (P = 1.84e−12; Fig. 1*B*). Forty-five of 59 (76.3%) tumors had *MET* levels greater than twice the mean of normal. Because primary pancreatic biopsies can vary widely in tumor content, and relative expression levels may vary with respect to tumor content, we further binned samples by tumor content (<10%, 10–25%, 25–50%, and 50–90%; Fig. 1). Again, there was a clear increase in the mean *HGF* or *MET* expression levels in all groups versus normal tissues. Although there seemed to be a trend of lower *HGF* levels in samples with high tumor content, this expression relationship was not statistically significant.

MetMAb inhibits HGF-dependent signal transduction and proliferation. To identify potential models of pancreatic cancer, seven pancreatic cancer cell lines were selected by relative *MET* and *HGF* expression and tested for responsiveness to HGF in proliferation assays (Supplementary Table S1). All lines responded to HGF with 1.2- to 3.2-fold increases in proliferation; two of which were selected for further analysis (Fig. 2*A*): BxPC-3 cells, expressing moderate levels of *MET* and responding to exogenous HGF with a 2.9-fold induction in proliferation, and KP4 cells, which express high levels of both *HGF* and *MET* in an autocrine manner. HGF-induced proliferation of BxPC-3 and KP4 was blocked with MetMAb at IC_{50}s of 8.73 and 5.0 nmol/L, respectively; however, KP4 cells were also sensitive to MetMAb in the absence of HGF (IC_{50}, 2.64 nmol/L), indicating that KP4 cells rely on active HGF/c-Met signaling for growth and survival (Fig. 2*A*).

Inhibition of KP4 cells by MetMAb was also associated with inhibition of c-Met phosphorylation and activation of several downstream pathway components. In KP4, c-Met was constitutively phosphorylated and was further elevated by adding exogenous HGF (Fig. 2*B*). MetMAb strongly inhibited c-Met and Gab-1 phosphorylation in a dose-dependent manner, resulting in 93% and 67% inhibition (1 μmol/L MetMAb, normalized to total β-actin), respectively (Fig. 2*B*). Likewise, MetMAb inhibited the phosphorylation of Akt, extracellular signal-regulated kinase (ERK) 1/2, and p70S6K (at 1 μmol/L) by 48%, 70%, and 32%, respectively (Fig. 2*B*). MetMAb also inhibited c-Met phosphorylation and downstream pathway activity in unstimulated KP4 cells to a similar extent as HGF-activated KP4 cells (Supplementary Fig. S1). These results show that MetMAb inhibits HGF-induced c-Met activation in paracrine- and autocrine-driven cell lines.

MetMAb inhibits BxPC-3 tumor xenograft growth in the human HGF osmotic pump model. Because mouse HGF does not activate human c-Met (30, 31), modeling ligand-driven activation of c-Met in animal tumor models requires either autocrine lines, such as KP4, or engineered paracrine models. We therefore sought to develop a novel *in vivo* model to grow BxPC-3 xenograft tumors in the presence of human HGF provided by implanted osmotic pumps. Human HGF pumps placed in the i.p. space led to high human HGF serum levels (in the 1–10 ng/mL range) with equivalent levels in each group (vehicle group mean = 3.8 ± 1.3 ng/mL; MetMAb group mean = 4.2 ± 1.3 ng/mL; Supplementary Fig. S2). Mice receiving human HGF pumps showed enhanced tumor growth compared with dextran sulfate pump and no pump control arms (Fig. 2*C*). Treatment of 140 mm^3 established BxPC-3 tumors in human HGF pump mice with MetMAb (30 mg/kg in 100 μL, i.p., twice weekly) resulted in significant inhibition of tumor

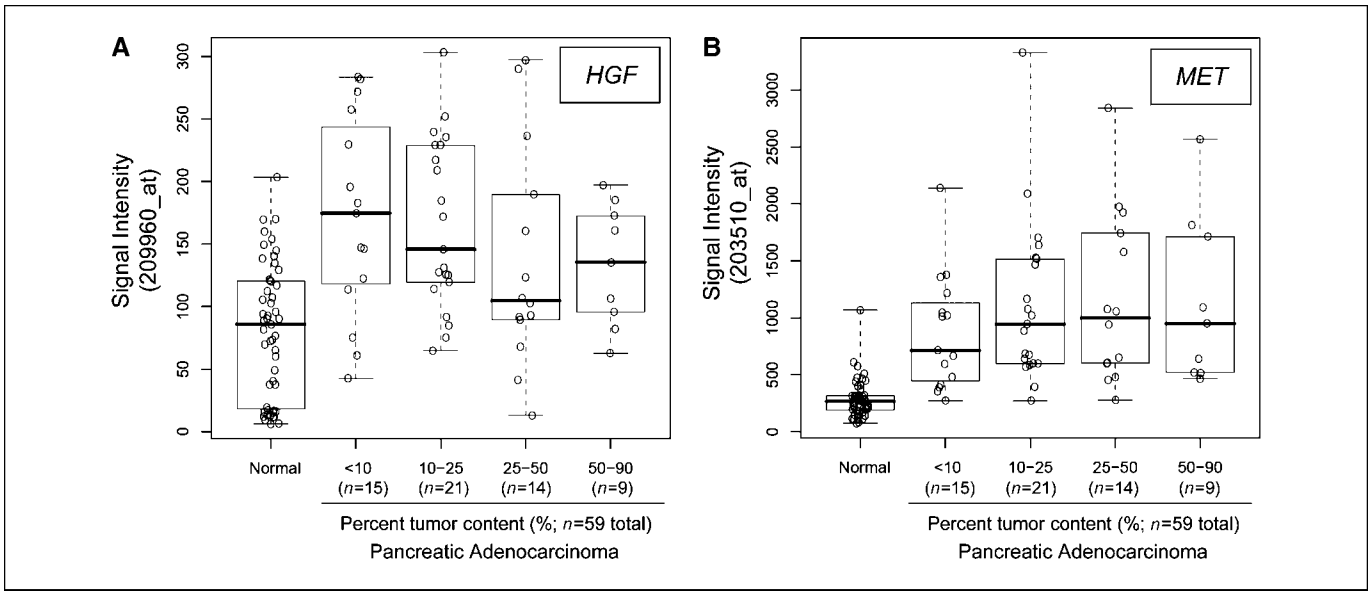

Figure 1. Analysis of *HGF* (*A*) and *MET* (*B*) gene expression in pancreatic tissues using microarray data. Multiple probe sets were found to match to each gene, and we chose 209960_at to represent *HGF* expression and 203510_at for *MET* because they gave relatively high signal intensities. *Y axes,* Affymetrix MAS5.0 signal intensity. *Open circle,* individual normal or adenocarcinoma sample. The box plot denotes 25th percentile, mean, and 75th percentile of each set of expression distribution. Pancreatic adenocarcinomas were binned by their percent tumor content with the number of tumors indicated/bin.

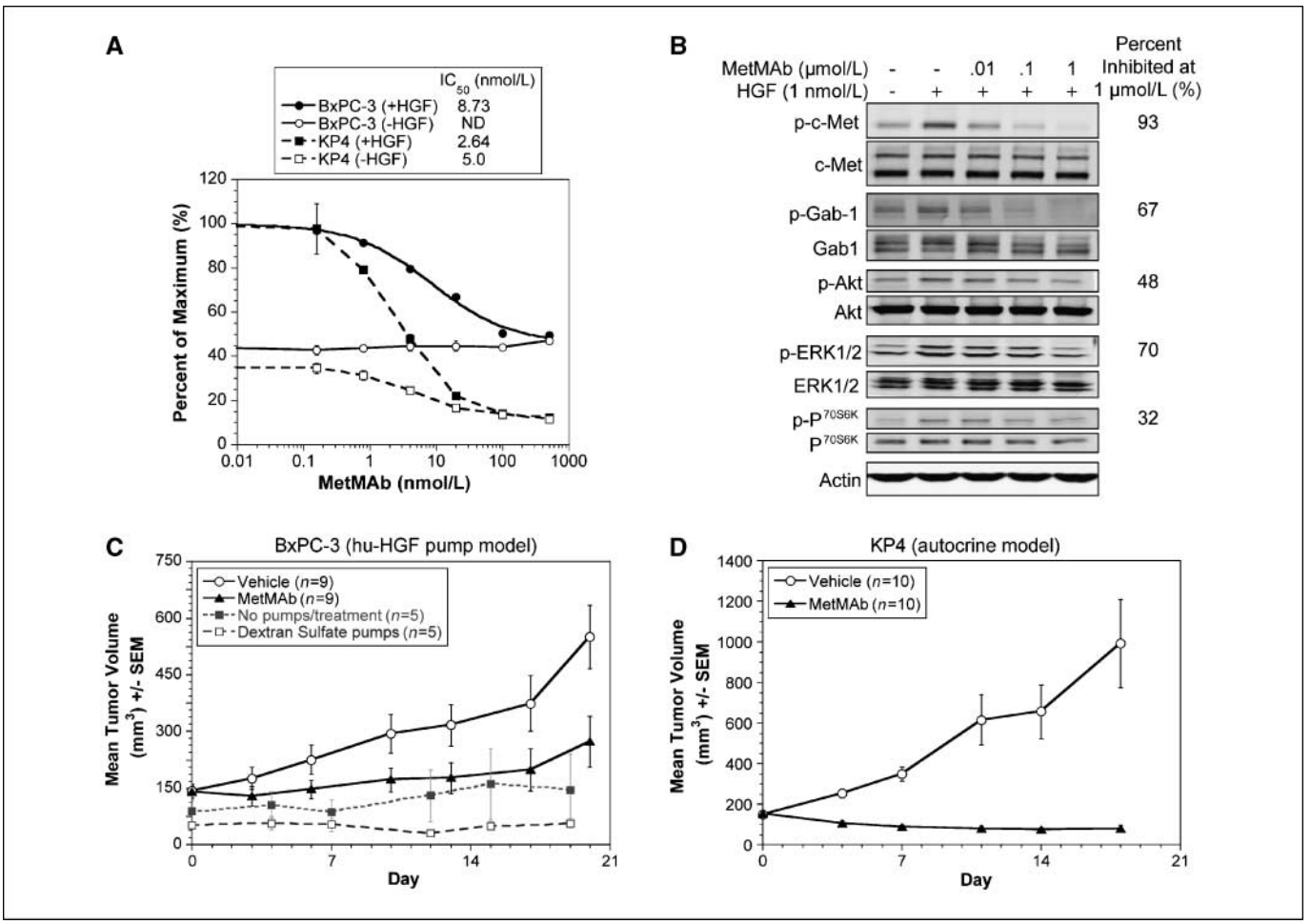

Figure 2. *A,* effect of MetMAb on cell proliferation in BxPC-3 (*circles with solid lines*) and KP4 (*squares with dashed lines*) pancreatic cancer cell lines in the presence (*filled symbols*) or absence (*empty symbols*) of HGF in Alamar Blue assays. IC_{50} values were calculated where possible and these are listed in the key. *B,* c-Met pathway analysis in KP4 cells treated with MetMAb at doses ranging from 10 nmol/L to 1 μmol/L. Total and phosphorylated signaling proteins were detected and quantified using LI-COR and normalized to β-actin with percent inhibition for phosphoproteins indicated on the right. *C,* MetMAb inhibits growth of established BxPC-3 xenografts in the human HGF osmotic pump model in nude (*nu/nu*) mice. The vehicle group (n = 9; *black empty circles, solid line*) received 5 million BxPC-3 cells a day after they were implanted i.p. with Alzet osmotic pumps containing human HGF (~2.4 mg/kg/d) in dextran sulfate, and were treated with vehicle. The MetMab group (n = 9, *black solid triangles, solid line*) was the same as vehicle group but treated with MetMAb (30 mg/kg, i.p., twice weekly). The no pump/treatment group (n = 5, *gray solid squares, dashed line*) received BxPC-3 cells as above, but without pumps and treatment. The dextran sulfate pumps group (n = 5, *gray empty squares, dashed line*) received BxPC-3 cells and pumps containing only dextran sulfate with no treatment. MetMAb has a significant effect on tumor growth (P = −0.02 on day 20). *D,* MetMAb substantially inhibits growth of established s.c. KP4 tumor xenografts in nude (*nu/nu*) mice. KP4 pancreatic tumors (n = 10 per group) received vehicle or MetMAb (30 mg/kg, i.p., twice weekly).

growth (P = 0.02 at day 20; Fig. 2*C*). These data show that MetMAb has antitumor activity in a pancreatic xenograft model driven by exogenous HGF.

MetMAb inhibits KP4 s.c. tumor xenograft growth. We next assessed the efficacy of MetMAb in the s.c. KP4 xenograft model. Tumors in vehicle-treated animals grew rapidly, whereas treatment with MetMAb (30 mg/kg in 100 μL, i.p., twice weekly) dramatically reduced tumor growth (Fig. 2*D*). These results show that KP4 is a HGF-dependent model and that MetMAb treatment can lead to tumor regressions used as a single agent when this tumor is grown s.c.

Effect of MetMAb on growth of orthotopic tumor xenografts. To generate models that better reflect pancreatic cancer, we developed an orthotopic model of KP4. The autocrine HGF/c-Met loop here allows for the evaluation efficacy of MetMAb in long-term survival studies a ligand-driven manner. Pilot studies showed that KP4 tumors seemed to grow within the pancreas, showing little local invasion to nearby organ sites. Following inoculation, KP4 tumors were allowed to grow for 12 days and then mice were grouped based on tumor volume measurements taken by micro-ultrasound imaging. Mice were treated with vehicle or MetMAb (30 mg/kg in 100 μL, i.p., twice weekly) for 2 weeks and then ultrasound imaging was carried out again to assess change in tumor volume.

Before treatment, there was no difference in mean tumor volume as measured by ultrasound in the two groups [8.34 ± 3.51 mm^3 (n = 19) in the vehicle group versus 8.63 ± 3.61 mm^3 (n = 20) in the MetMAb group]. Strikingly, ultrasound measurements taken following treatment showed that MetMAb abolished tumor growth (Fig. 3*A*). In vehicle-treated animals, mean tumor volume increased by ~92-fold compared with pretreatment tumor size, whereas tumor volume in MetMAb-treated mice decreased by −0.29-fold (Fig. 3*B*). Representative ultrasound images of one animal per group are shown in Supplementary Fig. S3*A*.

Effect of MetMAb treatment on survival in the KP4 orthotopic model. To test whether antitumor activity in the KP4 model translates into a survival benefit, treatment of the animals described above with vehicle or MetMAb (30 mg/kg in 100 μL, i.p., twice weekly) was continued for 11 weeks, and survival was followed for 90 days from study initiation. Continuous treatment with MetMAb for 11 weeks resulted in a substantial improvement in survival (Fig. 3*C*). Day 90 survival was increased by 424% in MetMAb-treated mice (55.0%) compared with vehicle controls (10.5%). Log-rank (Mantel-Cox) analysis of the plots showed significant survival benefit from treatment with MetMAb ($P = 0.0004$).

To assess whether short-term treatment could also result in a survival benefit in the KP4 orthotopic model, we conducted a survival study in which, 12 days after orthotopic injection of KP4 cells, mice were randomly grouped and treated with vehicle or MetMAb (30 mg/kg, i.p., twice weekly) for 2 weeks, and survival was followed for 90 days. Survival at the end point was 6 of 24 (25.0%) and 12 of 24 (50.0%), respectively, in the vehicle and MetMAb treatment groups (Fig. 3*D*). Survival benefit from treatment with MetMAb was statistically significant ($P = 0.0299$) as assessed by log-rank (Mantel-Cox) analysis of the plots. These data show that MetMAb significantly improves animal survival even when dosed for a shorter amount of time.

Effect of MetMAb on growth of larger orthotopic tumor xenografts. Because tumor size plays a role in determining therapeutic response, we next examined the effects of MetMAb treatment on growth of larger KP4 orthotopic tumors. For these studies, we increased both the number of injected KP4 cells (from 2 to 3 million) and the time for tumor growth before treatment initiation (from 12 to 16 days). These changes succeeded in increasing the mean tumor volume by ~5-fold compared with previous studies as measured by ultrasound and allowed for grouping out similarly sized tumors for MetMAb and vehicle treatment arms (49.7 ± 7.1 versus 49.5 ± 8.2 mm^3, respectively; $n = 13$ per group). Treatment was begun after 16 days with MetMAb (30 mg/kg, i.p., twice weekly) or vehicle for 2 weeks

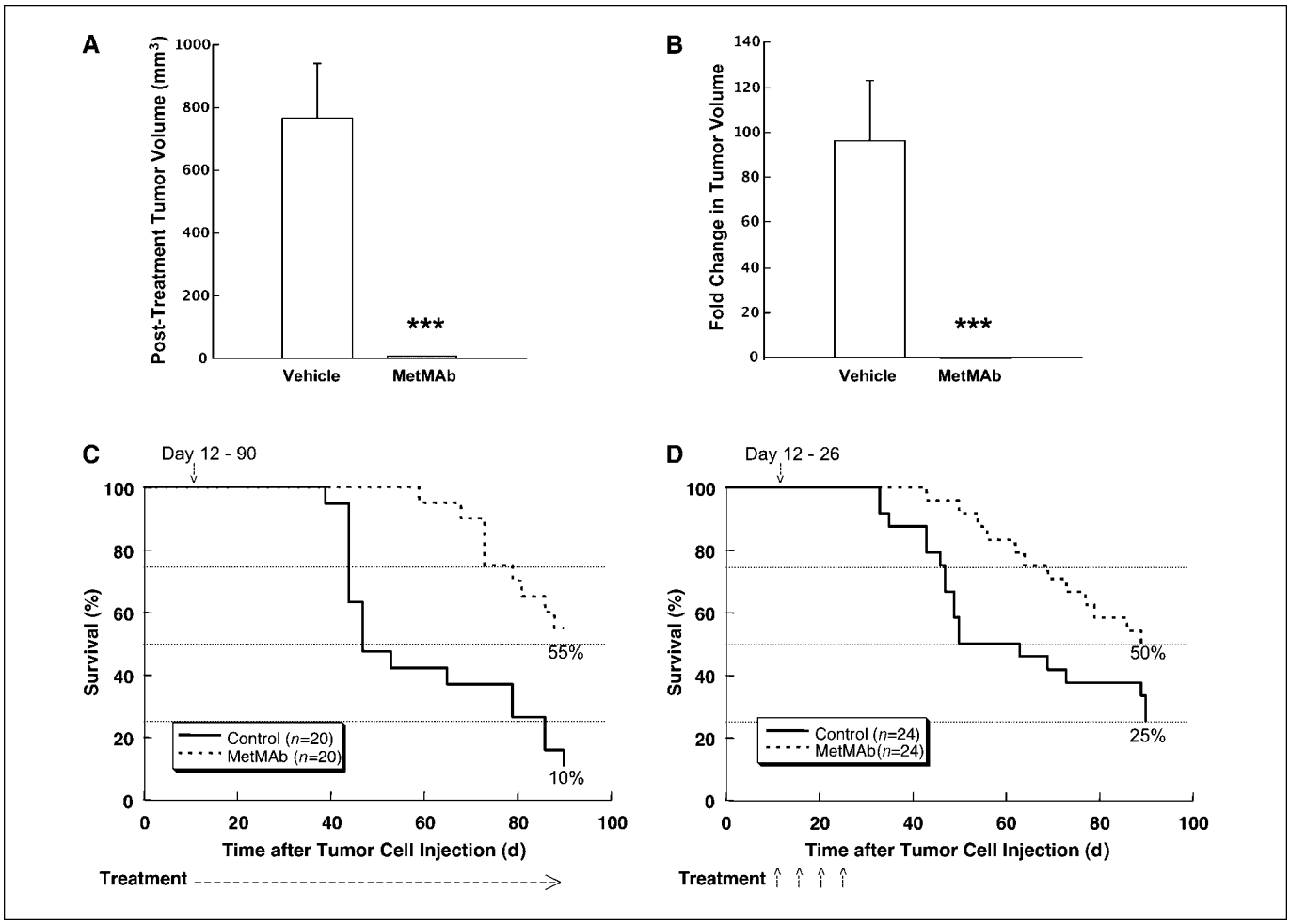

Figure 3. *A* to *C,* MetMAb shows strong antitumor activity in the KP4 orthotopic model of pancreatic cancer by ultrasound. Twelve days after intrapancreatic injection of KP4 cells, nude (*nu/nu*) mice received ultrasound imaging and were then treated with vehicle or MetMAb (30 mg/kg, i.p., twice weekly) for 2 wk. Ultrasound imaging was repeated 2 wk after treatment initiation. Treatment was continued for 11 wk, and survival was followed for 90 d after cell injection. Animal number was 19 to 20 in each group. There was no difference in tumor volume measured by ultrasound before treatment (8.34 ± 3.51 mm^3 and 8.63 ± 3.61 mm^3 in vehicle- and MetMAb-treated mice, respectively). *A,* tumor volume measured by ultrasound 2 wk after treatment initiation. *B,* fold change in tumor volume measured by ultrasound. ***, $P < 0.001$, between groups. *C,* effect of 11-wk treatment with MetMAb on survival. Log-rank (Mantel-Cox) comparison of survival plots indicated $P = 0.0004$ between the two group. *D,* effect of 2-wk treatment with MetMAb on survival in the orthotopic model of pancreatic cancer. Twelve days after intrapancreatic injection of KP4 tumor cells, nude (*nu/nu*) mice were treated with vehicle or MetMAb (30 mg/kg, i.p., twice weekly) for 2 wk, and survival was followed for 90 d after cell injection. Log-rank (Mantel-Cox) comparison of survival plots indicated $P = 0.029$ between treatment groups.

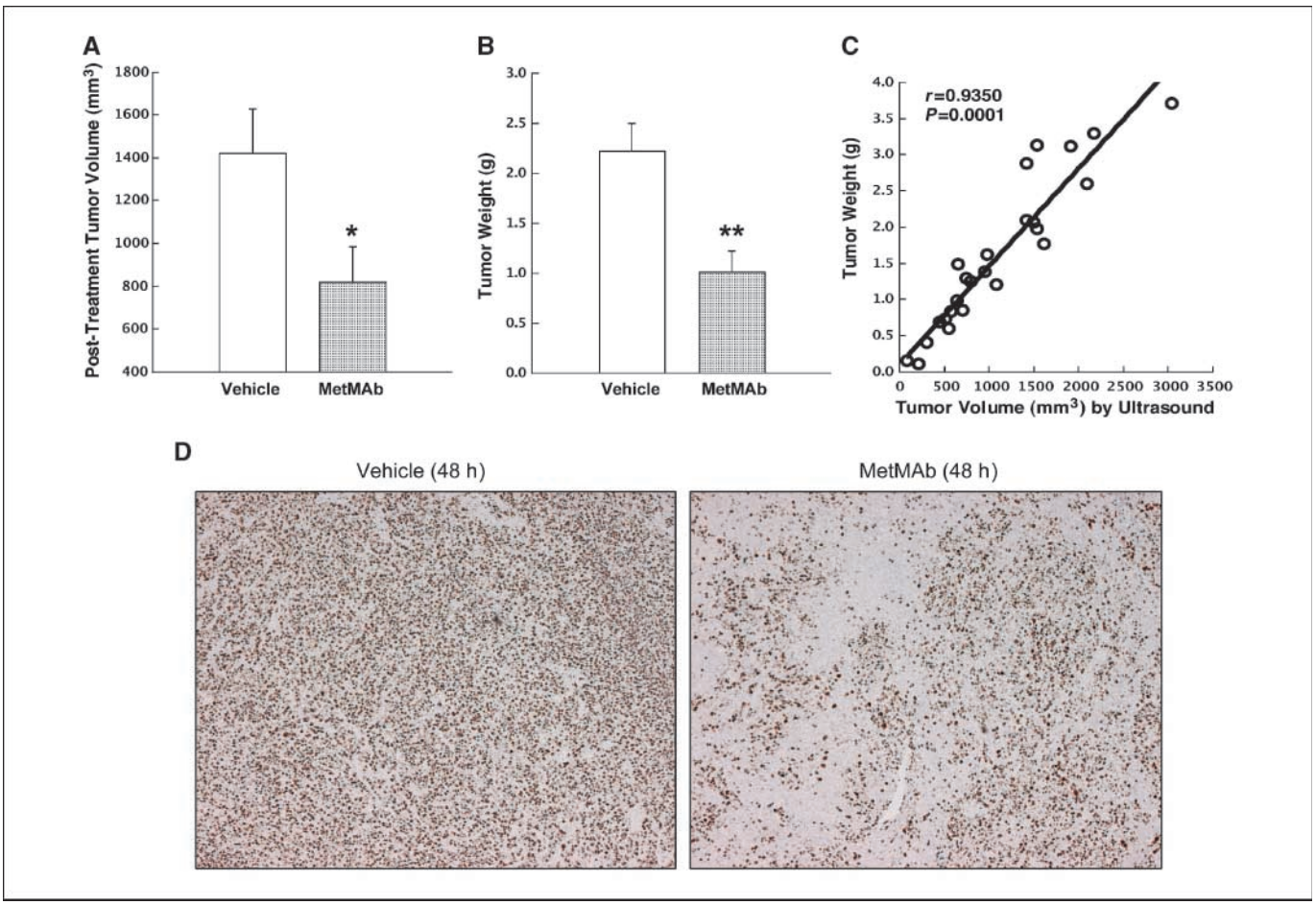

Figure 4. MetMAb inhibits the growth of large orthotopic KP4 pancreatic tumor xenografts. The amount of injected KP4 cells and the time for tumor growth before treatment were increased from 2 to 3 million cells and from 12 to 16 d after inoculation, respectively. Nude (*nu/nu*) mice received vehicle or MetMAb (30 mg/kg, i.p., twice weekly) for 2 wk (n = 12–13 per group). Ultrasound imaging of the pancreas was performed before and after treatment. The pancreas was removed, weighed, and saved for histologic studies after completing the second ultrasound examination. There was no difference in tumor volume measured by ultrasound before treatment (49.51 $\pm$ 8.22 mm^3 and 49.69 $\pm$ 7.11 mm^3 in vehicle- and MetMAb-treated mice, respectively). The increase in pretreatment tumor volume was ~5-fold over that in the above experiment (Fig. 3). *A,* tumor volume measured by ultrasound 2 wk after treatment initiation. *B,* mean tumor weights measured at necropsy. *, $P < 0.05$; **, $P < 0.01$, between groups. *C,* correlation between tumor volume measured by second ultrasound and tumor weight at necropsy. *D,* H&E staining tissue sections were stained with anti-Ki-67 antibody (clone SP6). The immunohistochemical images were taken at the median level of sectioning from one animal per group.

followed by ultrasound imaging and necropsy. MetMAb or vehicle was dosed over 14 days. Treatment was well tolerated as there was no difference in body weight between the two groups (30.67 $\pm$ 0.75 g versus 30.23 $\pm$ 0.63 g, respectively), although one animal in the vehicle group died before completing treatment. MetMAb treatment significantly inhibited tumor growth compared with vehicle as measured by ultrasound (817.5 $\pm$ 167.1 mm^3 versus 1,419.9 $\pm$ 205.1 mm^3, respectively; $P < 0.05$; Fig. 4*A*). The mean tumor volume in mice receiving vehicle increased by ~40-fold, whereas tumor growth was significantly reduced to ~18-fold in animals treated with MetMAb ($P < 0.05$). Furthermore, administration of MetMAb significantly diminished tumor weight compared with vehicle by 54% (1.02 $\pm$ 0.20 g versus 2.23 $\pm$ 0.27 g, respectively; $P < 0.01$; Fig. 4*B*). There was a high correlation between tumor volume measured by ultrasound and tumor weight (r = 0.935; P = 0.0001; Fig. 4*C*), indicating that ultrasound measurements are an accurate and reliable means for evaluating tumor responses in this model. Representative ultrasound images of one animal per group are shown in Supplementary Fig. S3*B*.

MetMAb inhibits KP4 proliferation *in vivo*. To address the potential mechanism of action of MetMAb on KP4 tumors, we determined if MetMAb inhibits tumor cell proliferation, as observed *in vitro*, by evaluating Ki-67 status (by immunohistochemistry) in KP4 orthotopic tumors treated with MetMAb (30 mg/kg, i.p., twice weekly) or vehicle for 2 weeks. The proliferative index, represented by Ki-67–positive nuclei, was clearly decreased in MetMAb-treated samples relative to those of vehicle-treated samples (Fig. 4*D*). MetMAb treatment resulted in a reduction in percentage of Ki-67–positive nuclei (52.5 $\pm$ 4.79% versus 85.0 $\pm$ 2.89%, respectively; n = 4 per group; $P < 0.01$). Evaluation of apoptosis induction was done in a separate study looking at response of s.c. KP4 tumors to single doses of MetMAb and the results from this showed little change in cleaved caspase-3 immunohistochemical staining (data not shown). This is consistent with data from U-87 MG (29) that showed that overall active caspase-3 is low and is only moderately affected by treatment with MetMAb (one-armed 5D5). These data suggest that the predominant effect of MetMAb in the KP4 autocrine model is antiproliferative.

MetMAb inhibits c-Met phosphorylation *in vivo*. To show that the antitumor effects of MetMAb are tied to inhibition of the c-Met pathway, studies were done to evaluate c-Met phosphorylation in

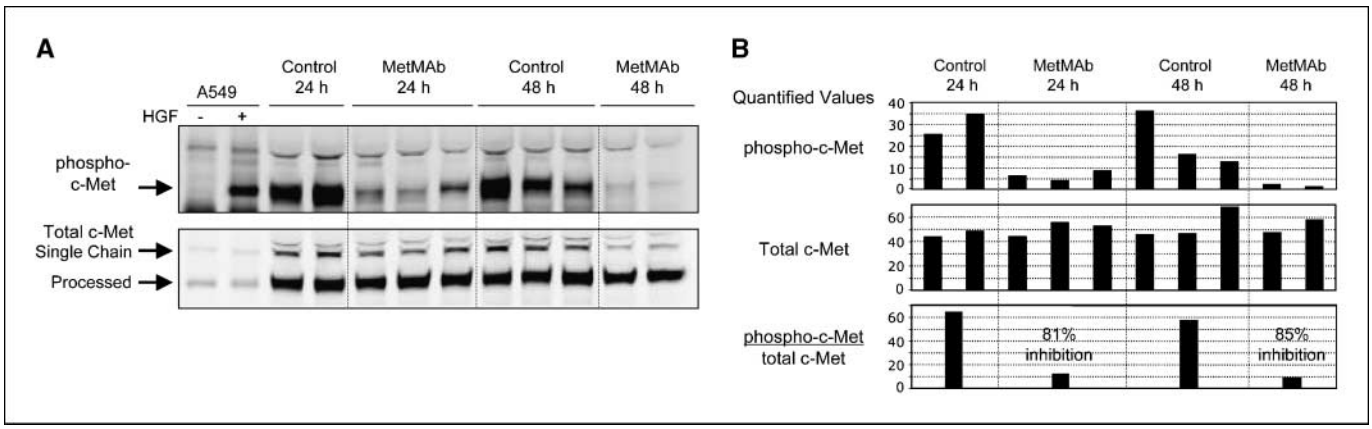

Figure 5. MetMAb inhibits c-Met phosphorylation in orthotopic KP4 tumors. KP4 orthotopic tumors were harvested at 24 and 48 h after a single dose of MetMAb (30 mg/kg, i.p.) or control (for each time point, $n = 2$ in the control group and $n = 3$ in the MetMAb group). *A,* tumor lysates were immunoprecipitated by anti-c-Met antibody (C-28) and blotted by anti-phosphotyrosine (4G10) and an anti-c-Met antibody (C-12). Cell lysates from A549 cells treated with or without 100 ng/mL HGF were loaded on the SDS gel as a positive control. *B,* the intensity of bands of phospho-c-Met (*top*) and total c-Met (*middle*) was quantified on a LI-COR Odyssey IR imaging system and the ratio of phospho-c-Met to total c-Met (*bottom*) from each tumor sample was used to evaluate c-Met phosphorylation. Tumor c-Met phosphorylation level in each treatment group was averaged. MetMAb treatment resulted in an 81% and 85% decrease in c-Met phosphorylation in KP4 orthotopic tumors at 24 and 48 h, respectively.

KP4 orthotopic tumors following 24 or 48 h after a single dose of vehicle or MetMAb (30 mg/kg). MetMAb reduced the ratio of phospho-c-Met to total c-Met by 81% at 24 h ($n = 2$ in the vehicle group, and $n = 3$ in the MetMAb) and 85% at 48 h ($n = 3$ in the vehicle group, and $n = 2$ in the MetMAb group) compared with vehicle-treated tumors (Fig. 5), indicating that MetMAb has a profound effect on KP4 c-Met phosphorylation within the pancreas.

Effect of MetMAb on tumor growth and angiogenesis in the dorsal skin window model. Activation of the c-Met pathway can lead to angiogenic responses either through direct activation of c-Met on endothelial cells or through release of angiogenic factors, such as the urokinase-type plasminogen activator (uPA) and the vascular endothelial growth factor (VEGF; ref. 36). Although we cannot address the role of c-Met on endothelial cells as MetMAb does not bind to mouse c-Met, indirect activation of angiogenesis was a potential mechanism of tumor growth that could be explored. Therefore, we sought to determine whether treatment of KP4 tumors with MetMAb results in an antiangiogenic response that could be discerned from the antiproliferative effects in a dorsal skin window model.

KP4 tumors were established by engrafting pieces of KP4 tumors grown s.c. Before treatment, tumor area in the dorsal window was similar in MetMAb-treated and vehicle groups (15.6 ± 2.2 mm^2 versus 15.3 ± 2.5 mm^2, respectively; $n = 4$ per group; Fig. 6*B*). The tumor area in the window of vehicle-treated mice progressively increased by 36.5% on day 3 (21.3 ± 4.2 mm^2), 185.9% on day 6 (44.6 ± 16.7 mm^2), and 259.0% on days 7 to 9 (56.0 ± 18.7 mm^2). In contrast, MetMAb treatment produced a substantial inhibition of tumor area with 14.7% reduction on day 3 (13.0 ± 2.7 mm^2), 47.5% on day 6 (8.0 ± 3.9 mm^2), and 71.9% on days 7 to 9 (4.3 ± 2.8 mm^2). There was a significant difference in the window tumor area between MetMAb- and vehicle-treated groups on days 6 and 10 ($P < 0.05$).

Tumor vascular density was measured by perfusing animals with FITC-dextran at various times after treatment and then directly imaging tumors via confocal microscopy. Before treatment, tumor vascular density was similar between the two groups (Fig. 6*D*). In contrast to its effect on tumor size, MetMAb did not cause a significant alteration in tumor vascular density (Fig. 6*D*). Representative tumor and tumor vascular images of animals from each group are shown in Fig. 6*A* and *C*, respectively. These results show that the predominant mechanism of activity of MetMAb in the KP4 model is through antiproliferative effects on KP4 tumor cells and not through secondary blockade of an angiogenic response.

Discussion

Expression of c-Met and HGF is correlated with tumor proliferation, invasive growth, and poor prognosis in multiple cancer types. In pancreatic cancer, we have shown that expression of *HGF* and *MET* is significantly up-regulated. These data are consistent with recent reports that show that HGF and c-Met also show higher protein expression by immunohistochemistry, which seems to be correlated with expression of hypoxia-inducible factor-1α and poor prognosis (37). Therefore, there is a need to generate models for this tumor type and to evaluate potential HGF/c-Met inhibitors. MetMAb, a potent anti-c-Met monovalent antibody, blocks HGF binding to c-Met and downstream activity. Although monoclonal anti-HGF/c-Met antibodies and MetMAb have shown efficacy in animal models of glioblastoma (27–29), we have shown here that MetMAb also has activity against both paracrine-driven (BxPC-3) and autocrine-driven (KP4) pancreatic tumor xenografts and that MetMAb treatment can significantly improve survival in the KP4 orthotopic pancreatic model.

As mouse HGF does not activate human c-Met (30, 31), the role of c-Met is not captured in typical mouse xenografts studies. Therefore, we developed the human HGF osmotic pump model that allowed us to grow BxPC-3 xenografts in a HGF-driven manner (Fig. 2*C*). Therein, MetMAb showed a statistically significant effect on the ability of BxPC-3 tumors to grow, indicating that MetMAb is capable of blocking HGF-enhanced paracrine signaling *in vivo* (Fig. 2*C*).

Identification of the KP4 autocrine pancreatic line was of great utility as it allows for the evaluation of HGF-driven tumor growth without the need for engineered paracrine models, making long-term survival studies more feasible. MetMAb showed great potency against s.c. grown KP4 tumors, indicating that this tumor is heavily dependent on HGF. To better model pancreatic cancer, we

developed the KP4 orthotopic pancreatic tumor xenograft model. Treatment of established tumors (~8.5 mm^3) with MetMAb completely abolished orthotopic tumor growth (Fig. 3*A* and *B*), consistent with the effects of MetMAb in s.c. models. However, because most patients with pancreatic cancer cannot be diagnosed at an early stage, we increased the pretreatment tumor size by ~5-fold to ~50 mm^3. Therein, MetMAb significantly inhibited tumor growth (Fig. 4*A* and *B*), although here we did not observe tumor regressions, rather only inhibition of tumor growth.

Survival is one of most important end points for preclinical and clinical studies on new anticancer therapies. Long-term (11 weeks) treatment with MetMAb substantially improved survival (P = 0.0004) as assessed by log-rank (Mantel-Cox) analysis (Fig. 3*C*), as did treatment with MetMAb for 2 weeks (P = 0.0299; Fig. 3*D*). The 90-day survival rate was increased by 100% after short-term treatment with MetMAb (12 of 24, 50.0%) versus vehicle (6 of 24, 25.0%), whereas long-term treatment enhanced 90-day survival rate by 424% (55.0% for MetMAb versus 10.5% for vehicle). Taken together, these results show the therapeutic potential of MetMAb in a ligand-driven pancreatic tumor model.

Promotion of invasive growth induced by HGF requires activation of multiple downstream signaling transduction pathways (38). HGF binding to the c-Met receptor induces dimerization and c-Met phosphorylation, activating various adaptor proteins, particularly Gab-1, leading to activity in multiple signaling pathways, including phosphatidylinositol 3-kinase (PI3K)/Akt, and the Ras/ERK and MAPK pathway, involved in inducing cell proliferation (39, 40). Activation of both PI3K/Akt and Ras/ERK signaling pathways stimulates p70S6K, contributing to HGF-induced invasion and migration (41). MetMAb markedly inhibited c-Met phosphorylation of KP4 tumor cells *in vitro* (Fig. 2) as well as in orthotopic KP4 pancreatic tumors (Fig. 5). Our *in vitro* studies also showed that inhibition of c-Met phosphorylation led to inhibition of Gab-1 and downstream PI3K/Akt, ERK1/2, and p70S6 phosphorylation. Furthermore, MetMAb treatment resulted in a dose-dependent inhibition of KP4 cell viability *in vitro*. Antiproliferative effects were recapitulated *in vivo* where MetMAb strongly decreased the Ki-67 proliferative index in orthotopic KP4 tumors. HGF and c-Met have been characterized as angiogenesis-promoting factors (36). HGF has been previously shown to act alone and in synergy with VEGF to induce growth of vascular growth (36, 42). Activation of tumor-expressed c-Met leads to expression of a wide variety of proteases and growth factors known to be involved in tumor angiogenesis, including uPA and VEGF. Treatment with MetMAb was associated with dramatic tumor regressions in the dorsal skin window model; however, this response was not accompanied by a

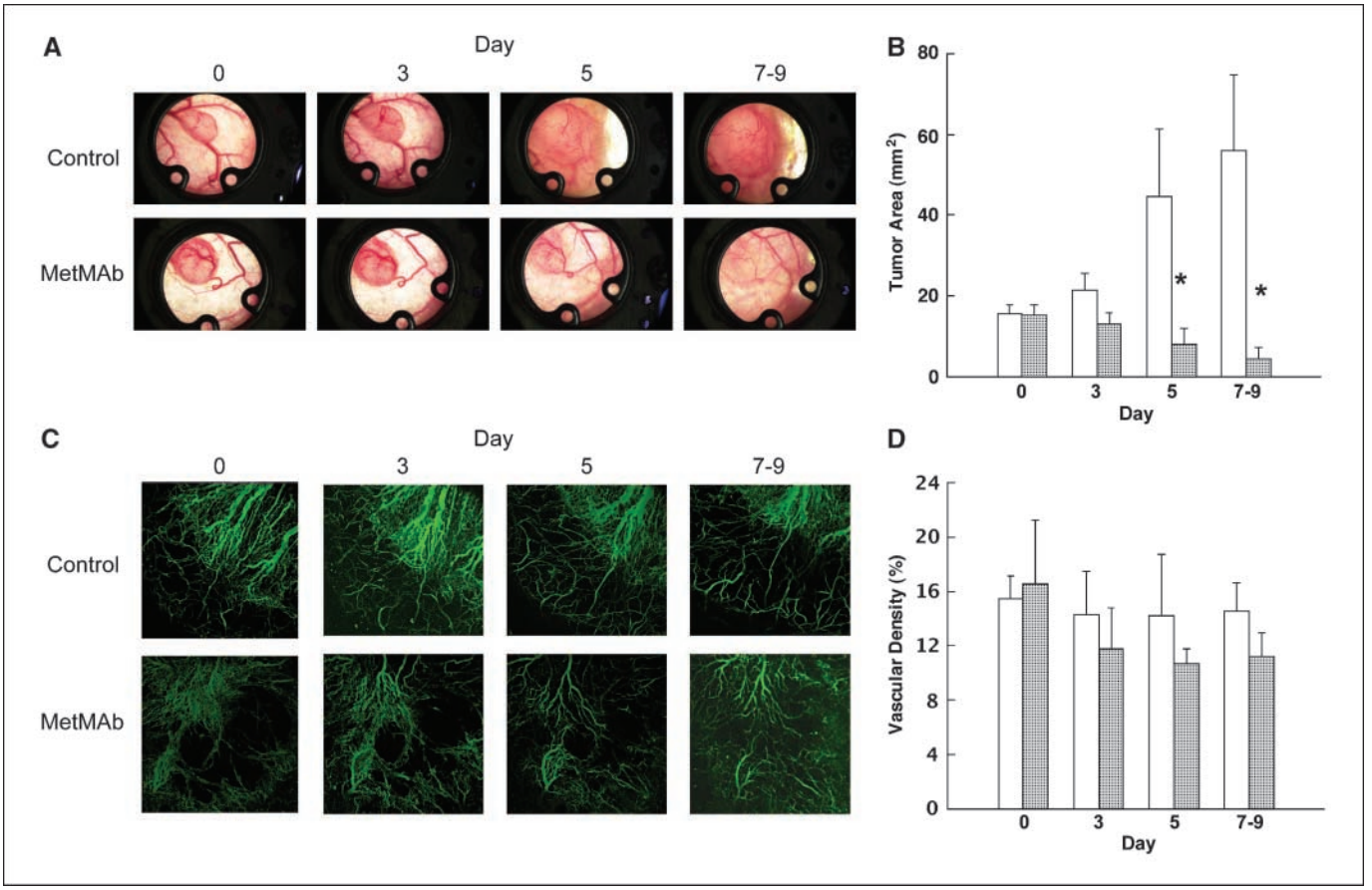

Figure 6. MetMAb shows antiproliferative but not antiangiogenic effects in the KP4 dorsal skin window model. A piece (~1 mm in diameter) of KP4 pancreatic tumor was implanted into the center of a dorsal skin window. When the window tumor reached ~4 mm in diameter, animals were treated with vehicle or MetMAb (30 mg/kg, i.p., twice weekly; n = 4 per group). Tumor size was monitored under light microscope, and tumor vessels were imaged by confocal microscopy after i.v. injection of FITC-dextran. *, P < 0.05, between the MetMAb-treated and vehicle groups at the same time point. *A,* representative light microscopic images of window tumor from one animal per group. *B,* effect of MetMAb on window tumor size under light microscope. *C,* representative confocal microscopic images of window tumor vessels labeled with i.v. infusion of FITC-dextran from one animal per group. *D,* effect of MetMAb on window tumor vascular density under confocal microscope. *White columns,* vehicle-treated; *shaded columns,* MetMAb-treated.

significant change in tumor vascular density (Fig. 6), suggesting that c-Met–dependent angiogenesis does not play a major role in KP4 tumor growth in mice. These observations show that MetMAb prevents HGF-induced activation of c-Met phosphorylation, thereby inhibiting downstream signaling activity and cellular responses, but in this setting does not seem to affect tumor angiogenesis. In conclusion, we have shown that, in HGF-driven models of pancreatic cancer, MetMAb shows potent antitumor efficacy and these data suggest that targeting HGF/c-Met in pancreatic cancer with MetMAb may have therapeutic potential for this deadly disease.

Disclosure of Potential Conflicts of Interest

All authors are employees of, and have ownership interest in, Genentech, Inc.

Acknowledgments

Received 10/22/2007; revised 3/4/2008; accepted 3/27/2008.

The costs of publication of this article were defrayed in part by the payment of page charges. This article must therefore be hereby marked *advertisement* in accordance with 18 U.S.C. Section 1734 solely to indicate this fact.

We thank Dr. Mark Sliwkowski for helpful suggestions, Mark Dennis for humanization of MetMAb anti-c-Met antibody, Nicholas Van Bruggen for imaging help, Bob Yanch for cell line microarray data, and J. Wang and Monique La Fleur for providing KP4 tumor cells.

References

1. Mancuso A, Calabro F, Sternberg CN. Current therapies and advances in the treatment of pancreatic cancer. Crit Rev Oncol Hematol 2006;58:231–41.
2. Michaud DS. Epidemiology of pancreatic cancer. Minerva Chir 2004;59:99–111.
3. Lowenfles AB, Maisonneuve P. Epidemiology and prevention of pancreatic cancer. Jpn J Clin Oncol 2004; 34:238–44.
4. Konner J, O'Reilly E. Pancreatic cancer: epidemiology, genetics, and approaches to screening. Oncology (Williston Park) 2002;16:1615–22.
5. Nakao AF, Fujii T, Sugimoto H, et al. Oncological problems in pancreatic cancer surgery. World J Gastroenterol 2006;12:4466–72.
6. Pasquali C, Sperti C, Filipponi C, Pedazzoli S. Epidemiology of pancreatic cancer in Northeastern Italy: incidence, respectability rate, hospital stay, costs, and survival. Digest Liver Dis 2002;34:723–31.
7. Nakamura T, Nawa K, Ichihara A. Molecular cloning and expression of human hepatocyte growth factor. Nature 1989;342:440–3.
8. Lokker NA, Mark MR, Luis EA, et al. Structure-function analysis of hepatocyte growth factor: identification of variants that lack mitogenic activity yet retain high affinity receptor binding. EMBO J 1992;11: 2503–10.
9. Naka D, Ishii T, Yoshiyama Y, et al. Activation of hepatocyte growth factor by proteolytic conversion of a single chain form to a heterodimer. J Biol Chem 1992; 267:20114–9.
10. Peruzzi B, Bottaro DP. Targeting the c-Met signaling pathway in cancer. Clin Cancer Res 2006;12:3657–60.
11. Christensen JG, Burrows J, Salgia R. c-Met as a target for human cancer and characterization of inhibitors for therapeutic intervention. Cancer Lett 2005;225:1–26.
12. Jiang WG, Martin TA, Parr C, Davies G, Matsumoto K, Nakamura T. Hepatocyte growth factor, its receptor, and their potential value in cancer therapies. Crit Rev Oncol Hematol 2005;53:35–69.
13. Bottaro DP, Rubin JS, Faletto DL, et al. Identification of the hepatocyte growth factor receptor as the c-met proto-oncogene product. Science 1991;251:802–4.
14. Naldini L, Vigna E, Narsimhan RP, et al. Hepatocyte growth factor (HGF) stimulates the tyrosine kinase activity of the receptor encoded by the proto-oncogene c-Met. Oncogene 1991;6:501–4.
15. Gao CF, Vande Woude GF. HGF/SF-Met signaling in tumor progression. Cell Res 2005;15:49–51.
16. Tomioka D, Maehara N, Kuba K, et al. Inhibition of growth, invasion, and metastasis of human pancreatic carcinoma cells by NK4 in an orthotopic mouse model. Cancer Res 2001;61:7518–24.
17. Bauer TW, Somcio RJ, Fan F, et al. Regulatory role of c-Met in insulin-like growth factor-1 receptor-mediated migration and invasion of human pancreatic carcinoma cells. Mol Cancer Ther 2006;5:1676–82.
18. Ebert M, Yokoyama M, Friess H, Buchler MW, Korc M. Coexpression of the *c-met* proto-oncogene and hepatocyte growth factor in human pancreatic cancer. Cancer Res 1994;54:5775–8.
19. Vila MR, Nakamura T, Real FX. Hepatocyte growth factor is a potent mitogen for normal human pancreas cells *in vitro*. Lab Invest 1995;73:409–18.
20. Furukawa T, Duguid WP, Kobari M, Matsuno S, Tsao MS. Hepatocyte growth factor and Met receptor expression in human pancreatic carcinogenesis. Am J Pathol 1995;147:889–95.
21. Kiehne K, Herzig KH, Folsch UR. c-met expression in pancreatic cancer and effects of hepatocyte growth factor on pancreatic cancer cell growth. Pancreas 1997;15:35–40.
22. Paciucci R, Vila MR, Adell T, et al. Activation of the urokinase plasminogen activator/urokinase plasminogen activator receptor system and redistribution of E-cadherin are associated with hepatocyte growth factor-induced motility of pancreas tumor cells overexpressing Met. Am J Pathol 1998;153:201–12.
23. Perugini RA, McDade TP, Vittimberga FJ, Callery MP. The molecular and cellular biology of pancreatic cancer. Crit Rev Eukaryot Gene Expr 1998;8:377–93.
24. Di Renzo MF, Poulsom R, Olivero M, Comoglio PM, Lemoine NR. Expression of the Met/hepatocyte growth factor receptor in human pancreatic cancer. Cancer Res 1995;55:1129–38.
25. Maehara N, Matsumoto K, Kuba K, Mizumoto K, Tanaka M, Nakamura T. NK4, a four-kringle antagonist of HGF, inhibits spreading and invasion of human pancreatic cancer. Br J Cancer 2001;84:864–73.
26. Ogura Y, Mizumoto K, Nagai E, et al. Peritumoral injection of adenovirus vector expressing NK4 combined with gemcitabine treatment suppresses growth and metastasis of human pancreatic cancer cells implanted orthotopically in nude mice and prolongs survival. Cancer Gene Ther 2006;13:520–9.
27. Burgess T, Coxon A, Meyer S, et al. Fully human monoclonal antibodies to hepatocyte growth factor with therapeutic potential against hepatocyte growth factor/c-Met-dependent human tumors. Cancer Res 2006;66: 1721–9.
28. Kim KJ, Wang L, Su YC, et al. Systemic anti-hepatocyte growth factor monoclonal antibody therapy induces the regression of intracranial glioma xenografts. Clin Cancer Res 2006;12:1292–8.
29. Martens T, Schmidt N-O, Eckerich C, et al. A novel one-armed anti-c-Met antibody inhibits glioblastoma growth *in vivo*. Clin Cancer Res 2006;12:6144–52.
30. Bhargava M, Joseph A, Knesel J, et al. Scatter factor and hepatocyte growth factor: activities, properties, and mechanism. Cell Growth Differ 1992;3:11–20.
31. Rong S, Bodescot M, Blair D, et al. Tumorigenicity of the met proto-oncogene and the gene for hepatocyte growth factor. Mol Cell Biol 1992;12:5152–8.
32. Wirtzfeld LA, Wu G, Bygrave M, et al. A new three-dimensional ultrasound microimaging technology for preclinical studies using a transgenic prostate cancer mouse model. Cancer Res 2005;65:6337–45.
33. Graham KC, Wirtzfeld LA, MacKenzie LT, et al. Three-dimensional high-frequency ultrasound imaging for longitudinal evaluation of liver metastases in preclinical models. Cancer Res 2005;65:5231–7.
34. Hoeflich KP, Gray DC, Eby MT, et al. Oncogenic BRAF is required for tumor growth and maintenance in melanoma models. Cancer Res 2006;66:999–1006.
35. Dennis MS, Jin H, Dugger D, et al. Imaging tumor with an albumin-binding Fab, a novel tumor-targeting agent. Cancer Res 2007;67:254–61.
36. Belle EV, Witzenbicher B, Chen D, et al. Potential angiogenic effect of scatter factor/hepatocyte growth factor via induction of vascular endothelial growth factor. Circulation 1998;97:381–90.
37. Ide T, Kitajima Y, Miyoshi A, et al. The hypoxic environment in tumor-stromal cells accelerates pancreatic cancer progression via the activation of paracrine hepatocyte growth factor/c-Met signaling. Ann Surg Oncol 2007;14:2600–7.
38. Comoglio PM. Pathway specificity for Met signaling. Nat Cell Biol 2001;3:E161–2.
39. Gahr S, Merger M, Bollheimer LC, et al. Hepatocyte growth factor stimulates proliferation of pancreatic β-cells particularly in the presence of subphysiological glucose concentrations. J Mol Endocrinol 2002;28:99–110.
40. Okano J, Shiota G, Matsumoto K, et al. Hepatocyte growth factor exerts a proliferative effect on oval cells through the PI3K/AKT signaling pathway. Biochem Biophys Res Commun 2003;309:298–304.
41. Zhou HY, Wong AST. Activation of p70S6K induces expression of matrix metalloproteinase 9 associated with hepatocyte growth factor-mediated invasion in human ovarian cancer cells. Endocrinology 2006;147: 2557–66.
42. Gerritsen ME, Tomlinson JE, Zlot C, et al. Using gene expression profiling to identify the molecular basis of the synergistic actions of hepatocyte growth factor and vascular endothelial growth factor in human endothelial cells. Br J Pharmacol 2003;140:595–610.

MetMAb, the One-Armed 5D5 Anti-c-Met Antibody, Inhibits Orthotopic Pancreatic Tumor Growth and Improves Survival

Hongkui Jin, Renhui Yang, Zhong Zheng, et al.

Cancer Res 2008;68:4360-4368.